JOM, Vol. 72, No. 2, 2020
https://doi.org/10.1007/s11837-019-03815-y
© 2019 The Minerals, Metals & Materials Society

PROGRESS WITH LEAD-FREE SOLDERS

Pressureless Silver Sintering of Silicon-Carbide Power Modules for Electric Vehicles

WON SIK HONG,[1,4] MI SONG KIM,[1] CHULMIN OH,[1]
YONGJIN JOO,[2] YOUNGSEOK KIM,[3] and KYOUNG-KUK HONG[3]

1.—Electronic Convergence Materials and Device Research Center, Korea Electronics Technology Institute (KETI), Seongnam-si, Gyeonggi-do 13509, Republic of Korea. 2.—Reliability Test Division, iA Powertron, Inc., Incheon 21314, Republic of Korea. 3.—Environment & Energy Research Team, Research & Development Division, Hyundai Motor Company, Hwaseong-si, Gyeonggi-do 16082, Republic of Korea. 4.—e-mail: wshong@keti.re.kr

Pressureless silver (Ag) sintering was optimized at 250°C in vacuum and nitrogen gas atmosphere with silicon carbide (SiC) chips, and silicon nitride active metal-brazed substrates (AMB). A 1200-V/200-A power module was developed using a pressureless Ag-sintered live SiC metal–oxide–semiconductor field-effect transistor (MOSFET) device and a Si_3N_4 AMB substrate module, and diverse reliability tests were performed. The void content and the bonding layer thickness of the Ag sinter joints were 1.2–3.4% and 68.5 μm. The bonding strength of the Ag sinter joints after thermal cycling testing (TCT) were slightly decreased due to the crack generation. In contrast, high-temperature storage testing (HTST) was carried out for a long time at high temperature, the sintering process occurred continuously, and the shear strength increased by 31% after HTST. The drain–source on-resistance ($R_{DS(ON)}$) of a SiC MOSFET power module before and after the TCT and power cycle test was similar to the as-sintered state without change.

INTRODUCTION

Various power modules have been developed to improve the power conversion efficiency of high-power devices. In particular, high heat resistance bonding technology has been actively studied along with a technology to replace conventional silicon chips with silicon-carbide (SiC) chips, which have wide band gaps.[1–4] SiC devices cannot use lead-free solder as a bonding material because of the temperature rise of 250°C due to the heat generated during operation; instead, gold (Au)-tin (Sn) or Au-based alloys must be used. However, because Au alloys are very expensive, it is inconvenient to commercialize these devices.[3,4] Therefore, silver (Ag) sintering and transient liquid phase (TLP) bonding technology are being studied as alternative bonding techniques.[1–8] Ag has a very high melting point of 961°C, enabling the use of heat-resistant solid-state sinter joints at very high temperatures. In addition, the Ag sinter bonding process can be carried out a temperature range of 200–250°C, which is lower than the melting point of Ag, under pressurized or pressureless conditions.[3,9] The pressurized sintering is a method of directly pressing the top surface of the device using a pressure jig during the sintering process in order to increase the densification of the sintered joint and lower the void content. However, the direct pressurization of the chip has the disadvantage of damaging the pattern on the top of the device. In addition, because several to several dozen power devices with several different thicknesses are sintered in one power module package, it is very difficult to pressurize all the chips at the same time while maintaining a constant thickness at a uniform pressure. Therefore, in consideration of mass production, a pressureless sintering process that is not directly pressurized during sintering is considered to be more advantageous.

The TLP bonding process has the advantage of utilizing existing lead-free soldering processes and equipment. TLP bonding is an interconnecting method in which a joint formed by using lead-free solder at a low temperature is transferred to an intermetallic compound (IMC) of Sn-Cu, Ag-Sn, or Ni-Sn systems, and can be safely used at high

temperatures without melting.[5–9] However, it is difficult to confirm the change of all joints into IMCs by nondestructive analysis methods, which is necessary for mass production. Therefore, considering current commercialization, the most suitable bonding method for SiC devices is the sinter joints process.[4–12]

When sintering is performed using an Ag paste with a SiC element, the material of the substrate is also very important. Because thermo-mechanical fatigue cracks are generated in the joint due to the warpage of the substrate, it is very important to use a substrate with small warpage, a coefficient of thermal expansion (CTE) similar to that of SiC, and an excellent heat dissipation property to improve the reliability of the module. The CTE of SiC is 2.7×10^{-6}/K, and the contents of alumina (Al_2O_3), AlN, and silicon nitride (Si_3N_4) are 6.7×10^{-6}/K, 4.5×10^{-6}/K, and 2.6×10^{-6}/K, respectively. Si_3N_4 is the most reliable substrate material because it has a CTE most similar to that of SiC and has a bending strength of approximately 800 MPa.[13]

In this study, a 1200-V/200-A metal-oxide semiconductor field-effect transistor (MOSFET) power module package for automobiles was developed using pressureless Ag sinter interconnection technology. The MOSFET module was assembled using a Ag-sintered SiC chip/Si_3N_4 active metal-brazed (AMB) substrate module, aluminum (Al) wire, copper (Cu) terminal, Cu base plate, and plastic case. Moreover, the pressureless Ag sinter bonding process was optimized at 250°C in a vacuum and nitrogen gas atmosphere using an Ag paste, SiC chips, and Si_3N_4 AMB substrates. The void maximum content of the sinter joint was 3.4%, and the initial shear strength, bonding layer thickness (BLT), and densification were 32.7 MPa, 68.5 μm, and 91.9%, respectively. To compare the reliability of the Ag sinter joints, thermal cycling tests (TCT), high-temperature storage tests (HTST), and power cycling tests (PCT) were conducted for 500 cycles, 700 h, and 1000 cycles, respectively.[14–16] After the TCT and HTST, the bond strengths were 25.7 MPa and 42.9 MPa, respectively and the densification was 90.3% and 95.4%, respectively. Furthermore, the bond strength after the HTST was higher. These results indicate that the sintering process is continuously generated during the long test at high temperature, and the densification of the joint is higher, which leads to an increase in the joint strength. The drain–source on-resistance ($R_{DS(ON)}$) was measured after the reliability tests. The $R_{DS(ON)}$ after the TCT and PCT tests was 6.63–6.97 mΩ, which was similar to the initial value of 6.60–6.99 mΩ. The microstructure and interface of the SiC chip/AMB substrate Ag-sinter joints were observed through scanning electron microscopy (SEM) and energy dispersive x-ray spectroscopy (EDS). The results confirmed that the commercialization of the sintered SiC chip/Si_3N_4 AMB substrate modules is feasible.

EXPERIMENTAL PROCEDURES

Ag Paste, SiC Device, and Si_3N_4 AMB Substrate

A commercial Ag paste (CT2700R7S; Kyocera Chemical, Japan) containing 90 wt.% Ag powder was used. Figure 1a and b shows photographs of the Ag-paste printed on a Si_3N_4 AMB substrate and the SiC chip mounted on the Ag-paste printed substrate before sintering. The SiC chips were used with a 1200-V/200-A and 25-mmΩ live MOSFET device (CPM2-1200-0040B; Cree, USA) and a SiC dummy die. The chip was 180 μm thick, 4.04 mm wide, and 6.44 mm long. The top and back were sputtered with Al (4 μm) and Ni (0.8 μm)/Ag (0.6 μm), respectively.

A Si_3N_4 AMB substrate with Ag finish was used. The substrate was 12.0 mm wide, 24.0 mm long, and 0.92 mm thick [0.3 (Cu)/0.32 (ceramic)/0.3 (Cu) mm]. The ZTA AMB substrate was composed of Al_2O_3 + ZrO_2 mixed ceramics (Amosense, Korea), and was 12.0 mm wide, 24.0 m long, and 0.72 mm thick [0.2 (Cu)/0.32 (ceramic)/0.2 (Cu) mm]. The base-plate material was C1220 Cu (90.0 mm × 45.0 mm, 3.0 mm thick), and had a thickness of 150 μm; a metal mask (stainless steel, SUS304) with a 70% printing area window was used.

Pressureless Ag-Sintering Condition

Figure 1c and d shows the vacuum bonding furnace (Ajeon-010; Ajeon Heating Industrial, Korea) used for the pressureless Ag sintering process. Figure 1e shows the temperature and pressure profiles of the pressureless sintering process. The sintering was carried out at 250°C without pressure in vacuum and nitrogen atmosphere for 90 min.

Reliability Test Conditions

To compare the reliability of the sinter joints before and after Ag sintering, TCTs, HTSTs, and power cycling tests were conducted. The 1200-V/200-A SiC MOSFET power modules were utilized for the reliability tests, with samples assembled using an Ag-sintered SiC chip/Si3N4 AMB substrate module, aluminum wire, Cu terminal, and Cu base plate with a plastic case, as shown in Fig. 2.

The TCT temperature ranged between − 50°C and 150°C (ΔT = 250°C) with a soak time of 10 min for 500 cycles using a thermal cycling chamber (TSA-11A; Espec, Japan). The HTST was carried out at 200 ± 3°C for 700 h using a high-temperature storage oven (OF-22GW; Jeio Tech, Japan). Power cycling was carried out at 50–100°C (ΔTc = 50°C) and 1–6 min dwell time at each

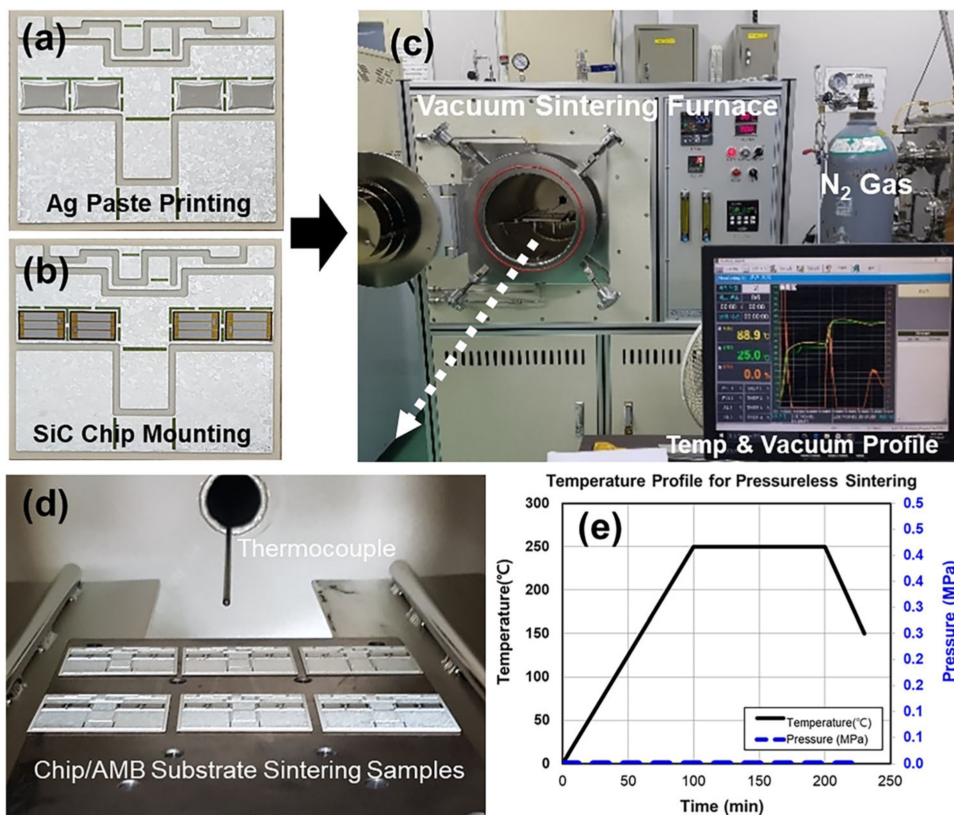

Fig. 1. Photographs of pressureless sintering process: (a) Ag-paste printing on a Si_3N_4 AMB substrate, (b) SiC chip mounting on an Ag-paste printed substrate, (c, d) pressureless sintering machine set-up and samples, respectively, and (e) temperature and pressure profiles for Ag sintering.

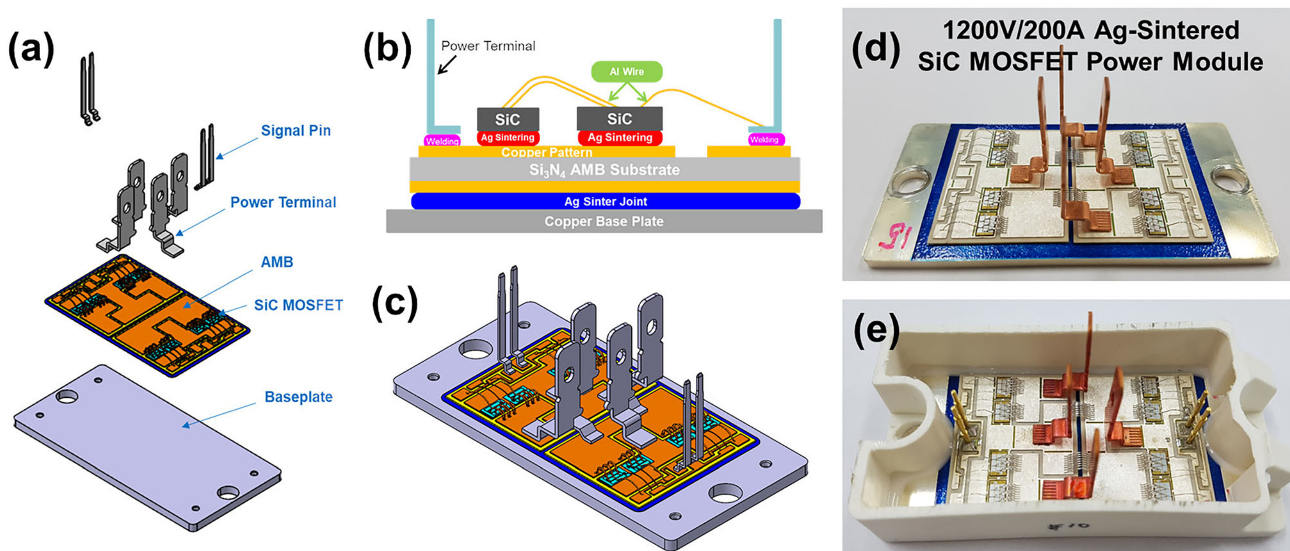

Fig. 2. Schematic diagrams of (a) components, (b) cross-sectional structure, (c) before case molding assembly, and photographs of (d) before and (e) after plastic case molding assembly.

temperature for 1000 cycles, as shown in Fig. 3, using a power cycling test machine (Ontest, Korea). The test method of power cycling for the 1200-V/200-A SiC MOSFET modules was carried out according to the JEDEC standards: 20 V applied at the gate and then 160 A applied at the low side, and once the device's temperature reached 150°C, the power supply was stopped and allowed to cool until the temperature of the case was 50°C. This procedure was repeated for 1000 cycles.[16] After finishing each reliability test, the $R_{DS(ON)}$ was measured with a power device analyzer for circuit design (B1506A; Keysight Technologies, USA).

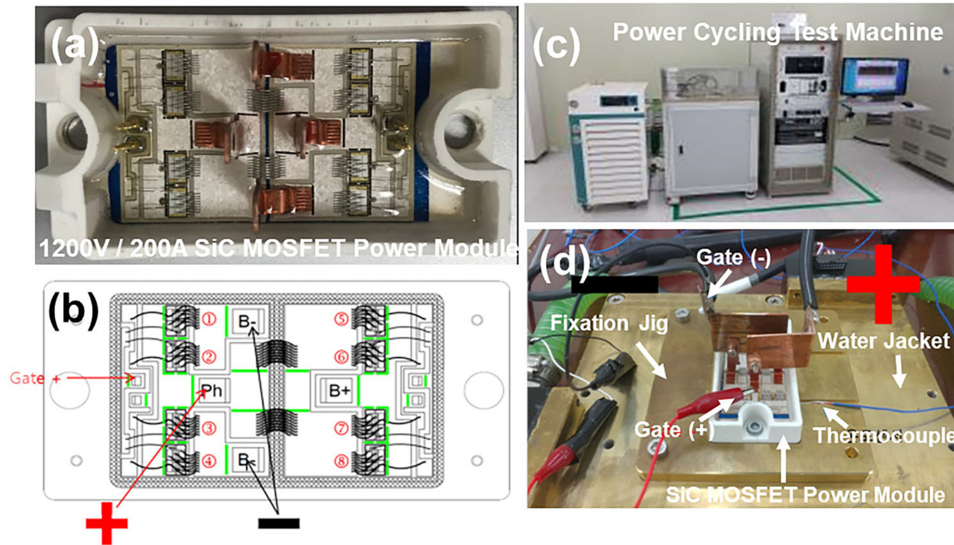

Fig. 3. Photographs of the power cycling test: (a) pressureless Ag-sintered 1200-V/200-A SiC MOSFET power module, (b) schematic of the test process, (c) power cycling test machine, and (d) power cycling test.

Densification Measurement of Ag-Sinter Joints

After the pressurized sintering, the cross-sectional area of the Ag-sinter joints was examined. The cross-sectional morphology was obtained and the porosity of the Ag sinter joints was measured using the *i*-solution software (Image & Microscope Technology, USA). The densification of the Ag-sinter joints was calculated as the ratio of the porosity to the sinter joint area.

RESULTS AND DISCUSSION

Void Content and Shear Strength of Pressureless Ag-Sintered SiC Chip/Si_3N_4 AMB Substrate Joints

Figure 4a shows a photograph of the pressureless Ag-sintered SiC Chip/Si_3N_4 AMB substrate sample and Fig. 4b and c are non-destructive x-ray analysis images. The void content was 1.2–3.4% of the sinter joint layer, which was the average of the three samples.

Figure 4d compares the void content and the shear strength before and after the TCT and HTST. The bond strength of the SiC chip/Si_3N_4 substrate of the as-sintered sample was 32.7 MPa and the void content was 4.1%. After the TCT, the bond strength decreased to 25.7 MPa and, after the HTST, it increased to 42.9 MPa, compared with the as-sintered value. The void contents were 5.0% and 3.3% after the TCT and HTST, respectively. It should be noted that a void content of 10% or less is acceptable for mass production. Because a high temperature was continuously maintained during the HTST, the Ag sintering process occurred, which led to the increase in the shear strength of the Ag sinter joints. However, the TCT caused a mismatch of the coefficient of thermal expansion (CTE) in the sinter joints; finally, the bonding strength was decreased after the TCT. Therefore, the TCT is more effective than the HTST for evaluating the sinter joints.

Bonding Layer Thickness, Densification, and Microstructure of Pressureless Ag-Sinter Joints

Figure 5a–c shows the cross-sectional SEM micrographs used to measure the BLT and densification of the Ag sinter joints after the TCT and HTST compared with the as-sintered state, and Fig. 5d shows the measurement results of the BLT and the densification. As shown in Fig. 5d, the initial BLT of the Ag-sinter joints was 68.5 μm; after the TCT and HTST, the BLT was 68.4 μm and 75.1 μm, respectively.

The initial densification of the Ag-sinter joint measured from Fig. 5a–c was 91.9%, and, after the TCT and HTST, it was 90.3 and 95.4%, respectively. The densification remained similar after the TCT, whereas it increased after the HTST, similar to the void content. Because the TCT can generate thermo-mechanical fatigue cracks at the Ag-sinter joints due to the CTE, the densification after the TCT was similar or lower than the initial one. Similar to the principle of void reduction after the TCT, the densification also increased after the test. The densification increased because the HTST was applied at a high temperature for a long time, so that sintering based on the solid-state diffusion bonding occurred continuously during the test.

Figure 6 shows SEM images of the (a) as-sintered SiC chip/ZTA AMB substrate joint and (b–d) magnified images. It was confirmed that the sinter joint was densely bonded. In addition, it can be seen that sintering was successfully performed at the interface between the back side of the SiC chip with the

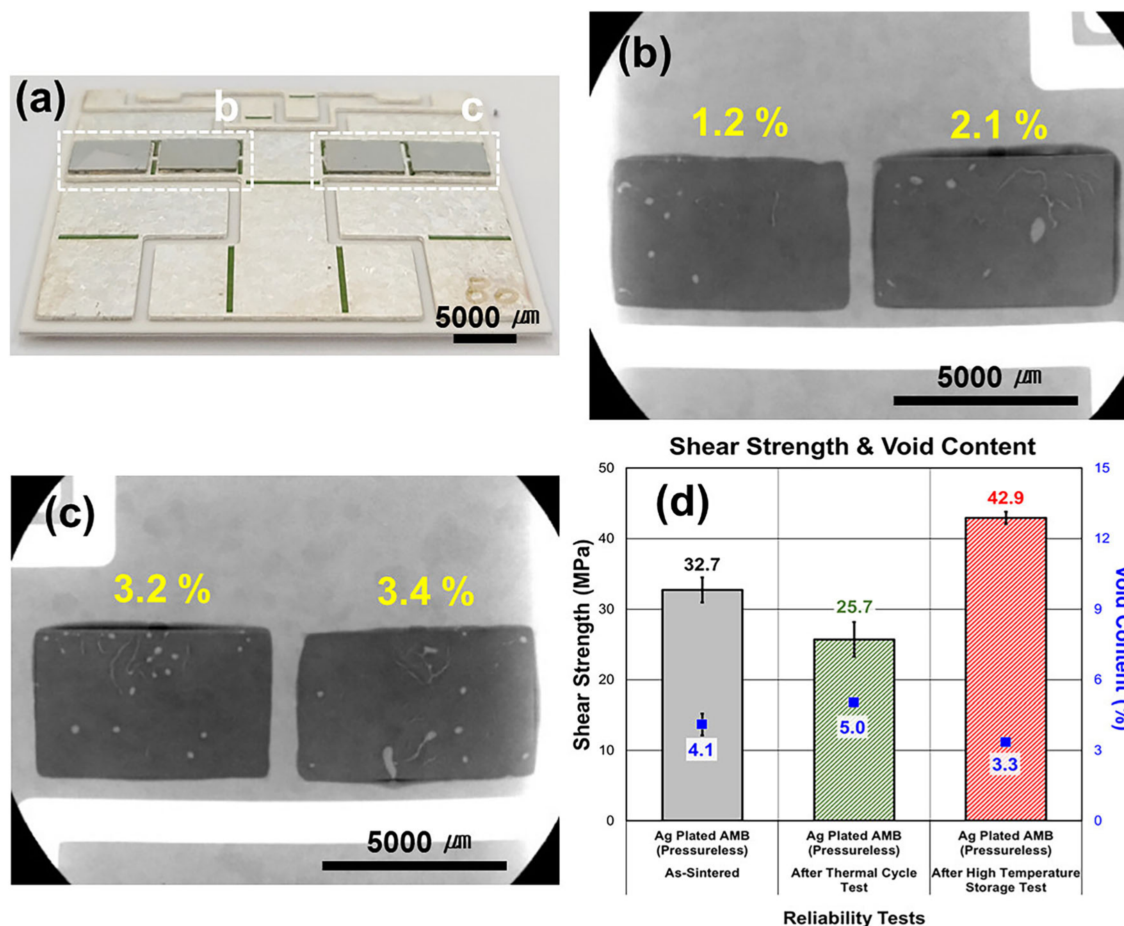

Fig. 4. (a) Photograph of pressureless Ag-sintered SiC chip/AMB substrate module, (b, c) non-destructive x-ray analysis images, and (d) a graph of shear strength and void content comparison of Ag sinter joints before and after the TCT and the HTST.

Ag-coated surface and the Ag paste. In particular, an Ag-Cu alloy layer was formed at the interface between the Ag sinter matrix and the Ag-finish surface of the substrate.[17,18] This Al-Cu alloy layer is considered to be formed by inter-diffusion between the Cu layer and the Ag coating layer of the substrate.[17,18] In the Ag-sinter joint, it was observed that the network structure formed between the powders was sufficient to reach a densification of 91.9%. During the sintering process of the solid state, the network formation process of the Ag powders is carried out through the original point contact, neck growth, pore-channel closure, pore rounding, densification and pore shrinkage, and pore coarsening.[3,17,19–22] When these sintering processes are successfully performed, the densification can be 90% or more.

Figure 7a shows SEM images of the Ag sinter joint of the SiC chip/AMB substrate after the TCT. Figure 7b–d shows an enlarged view of the left side and the AMB substrate side of the SiC chip, and the sintered-Ag matrix, respectively. Figure 7b and c shows that cracks are generated in the sinter joint due to the repeated thermo-mechanical stress during the TCT induced by the difference in CTE between the SiC, sintered-Ag, and substrate. The shape of the crack indicates a typical fatigue crack.[23] The pores were observed in a grain, and some voids existed at the triple point of particles. Figure 7d shows the microcrack evolution at the triple contact points of the Ag-sinter joint due to the thermal fatigue during the TCT. The microcracks were mainly observed at the triple contact point of the particles. The triple contact points around the pores or voids were in the continuous sintering process, those areas acting as a fracture site where cracks could occur. As the operation progressed, these microcracks propagated inside the sinter joint and the bond strength decreased.

$R_{DS(ON)}$ of SiC MOSFET Power Module After the Power Cycling

Figure 8 shows SEM images of the 1200-V/200-A SiC MOSFET power module Ag-sinter joints after the PCT for 1000 cycles and after the TCT for 500 cycles were compared to those in the as-sintered state. The $R_{DS(ON)}$ of SiC MOSFET power module was measured before and after the reliability tests.

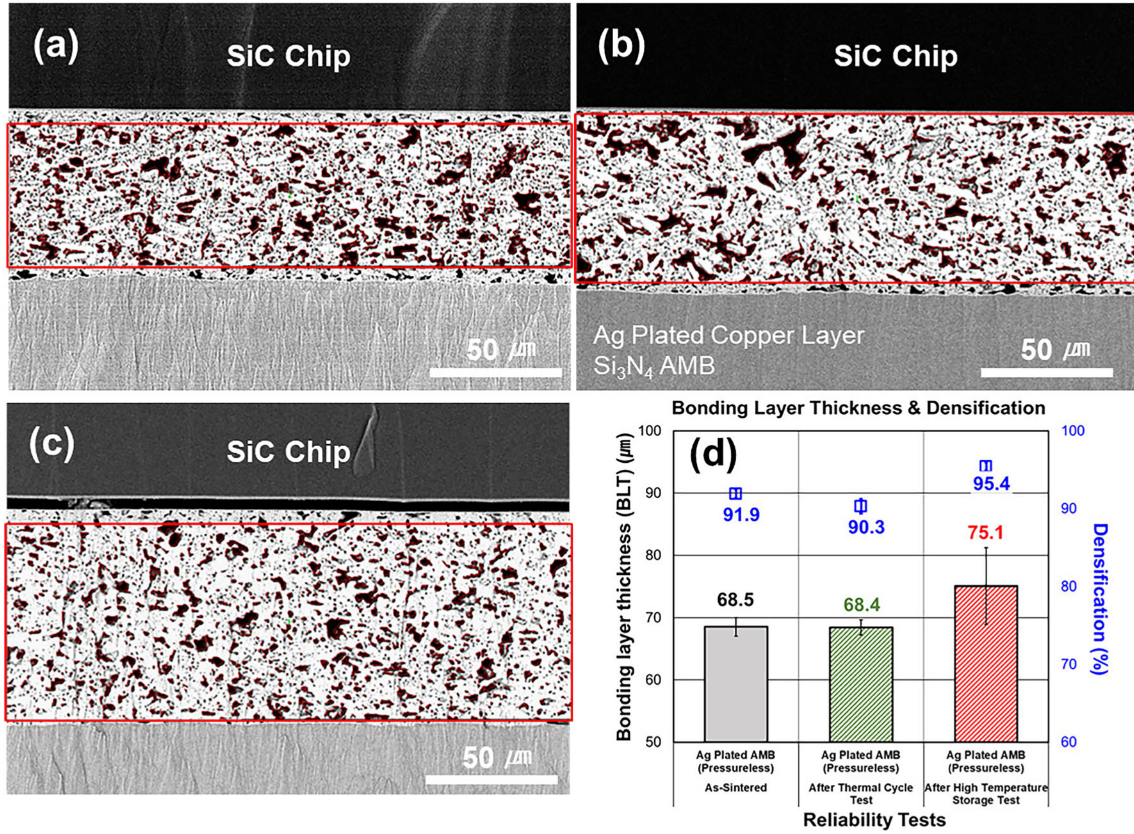

Fig. 5. Cross-sectional SEM micrographs for measuring the bonding layer thickness and densification of the pressureless Ag-sinter joints: (a) as-sintered, (b) after 500 thermal cycles, and (c) after 700 h high-temperature storage; and (d) BLT and densification measurement results.

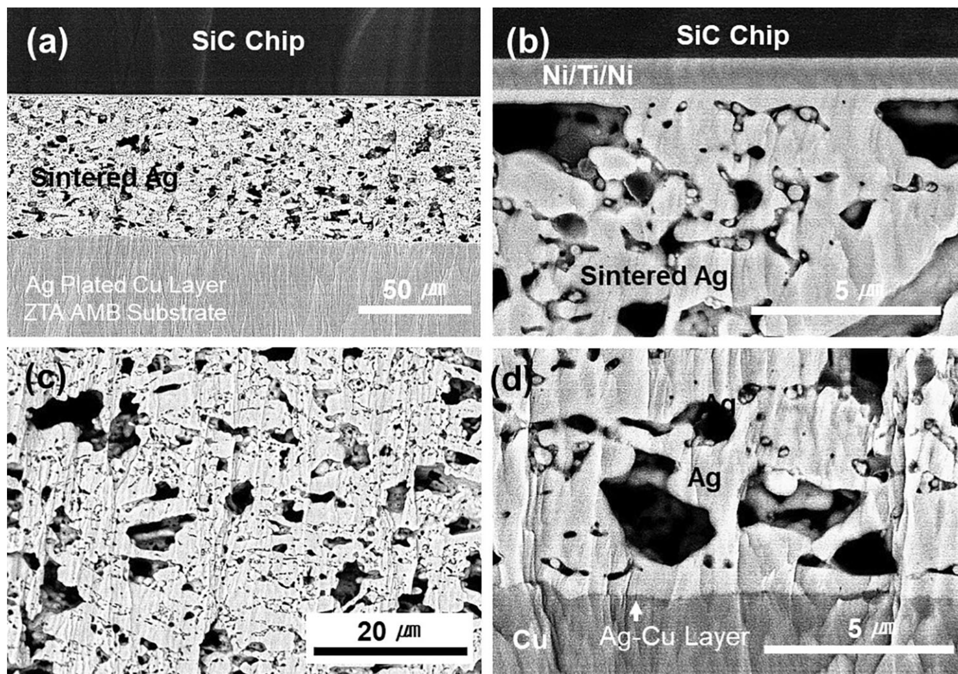

Fig. 6. SEM images of (a) as-sintered SiC chip/ZTA AMB substrate joint and a magnified view of (b) SiC die side, (c) Ag sinter joint, and (d) substrate side.

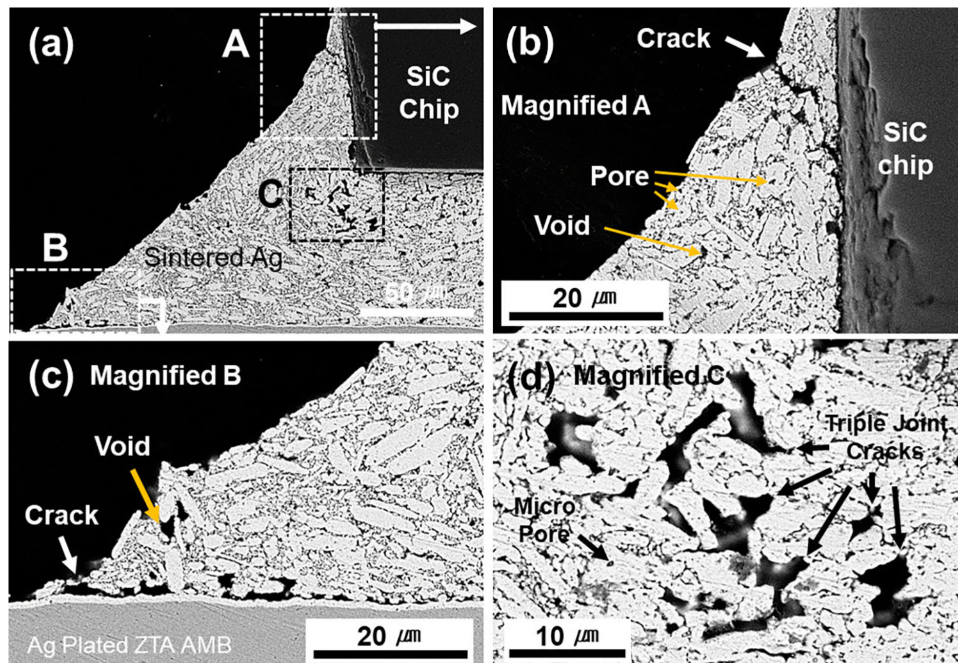

Fig. 7. SEM images of (a) Ag sinter joint of SiC chip/AMB substrate after the TCT. Enlarged views of (b) the left side, (c) the AMB substrate side of the SiC chip, and (d) the sintered Ag, respectively.

The $R_{DS(ON)}$ represents the total resistance in the path between the drain and source in a MOSFET module and consists of a number of resistances. Because the sinter joint is bonded to the SiC chip, its resistance is included in $R_{DS(ON)}$. Therefore, if a defect occurs in the Ag-sinter joints, the on-resistance will increase. The $R_{DS(ON)}$ is the basis for the maximum current rating of the MOSFET and is also associated with current losses. Thus, the power conversion efficiency of the power module is increased when the $R_{DS(ON)}$ is reduced. Finally, it is important to observe the change in the $R_{DS(ON)}$ to observe the bonding state of the module.

The $R_{DS(ON)}$ specification of the 1200-V/200-A SiC MOSFET device was 8 mΩ and the initial $R_{DS(ON)}$ was 6.60–6.99 mΩ. After the TCT and PCT, the $R_{DS(ON)}$ was 6.77–6.92 Ω and 6.63–6.97 Ω, respectively. These results indicated that, after the reliability test, the $R_{DS(ON)}$ remained constant during module operation, which in turn indicates that the sinter joint was well maintained.

The magnified SEM images of the SiC chip side and the Si_3N_4 AMB substrate side indicated that the sinter joint was well formed in the as-sintered joints and that the network microstructure was maintained after the PCT and the TCT.

The densification of the sinter joints after PCT and TCT was similar, and cracks were not observed. The PCT test drives the device directly to maintain high and low temperatures, thus applying the worst drive conditions to the sinter joints of the chip. On the other hand, because the TCT test applies heat to the entire module, more stress is applied to a larger area, such as a substrate or a base plate, in addition to the chip joint, so that a crack occurs more rapidly. For these reasons, the PCT test is suitable for evaluating the reliability of the die attachment joint, and the TCT test is suitable for verifying the reliability of a large-area joint. Comparing the microstructures of the SiC chip/Ag powder sinter joints in Fig. 8, the porosity or micro-pores of the sinter joints after the PCT test can be seen to be larger and higher in the PCT test samples than the TCT samples. This is because the PCT test induces more severe conditions for the sinter joints, as the device is directly driven to generate heat.

CONCLUSION

Pressureless Ag sintering was optimized using a SiC chip on a Si_3N_4 AMB substrate at 250°C for 90 min without pressure in a vacuum and nitrogen atmosphere. The void content and shear strength of the SiC chip/AMB substrate sinter joints were 3.3–5.0% and 32.7 MPa, respectively. The BLT of the pressureless Ag sinter joint was maintained at a constant thickness of 68.4–75.1 μm. To evaluate the sinter joint reliability, the shear strength, BLT, and densification were measured after the TCT and HTST. The shear strengths were 25.7 MPa and 42.9 MPa after the TCT and HTST, respectively. The shear strength after the HTST was increased compared to the initial strength. Because sintering progresses continuously during the HTST, the densification of the sinter joints increased to 95.4%, which caused an increase in the shear strength. The microcracks were generated at the Ag-sinter joint due to the thermal fatigue during the

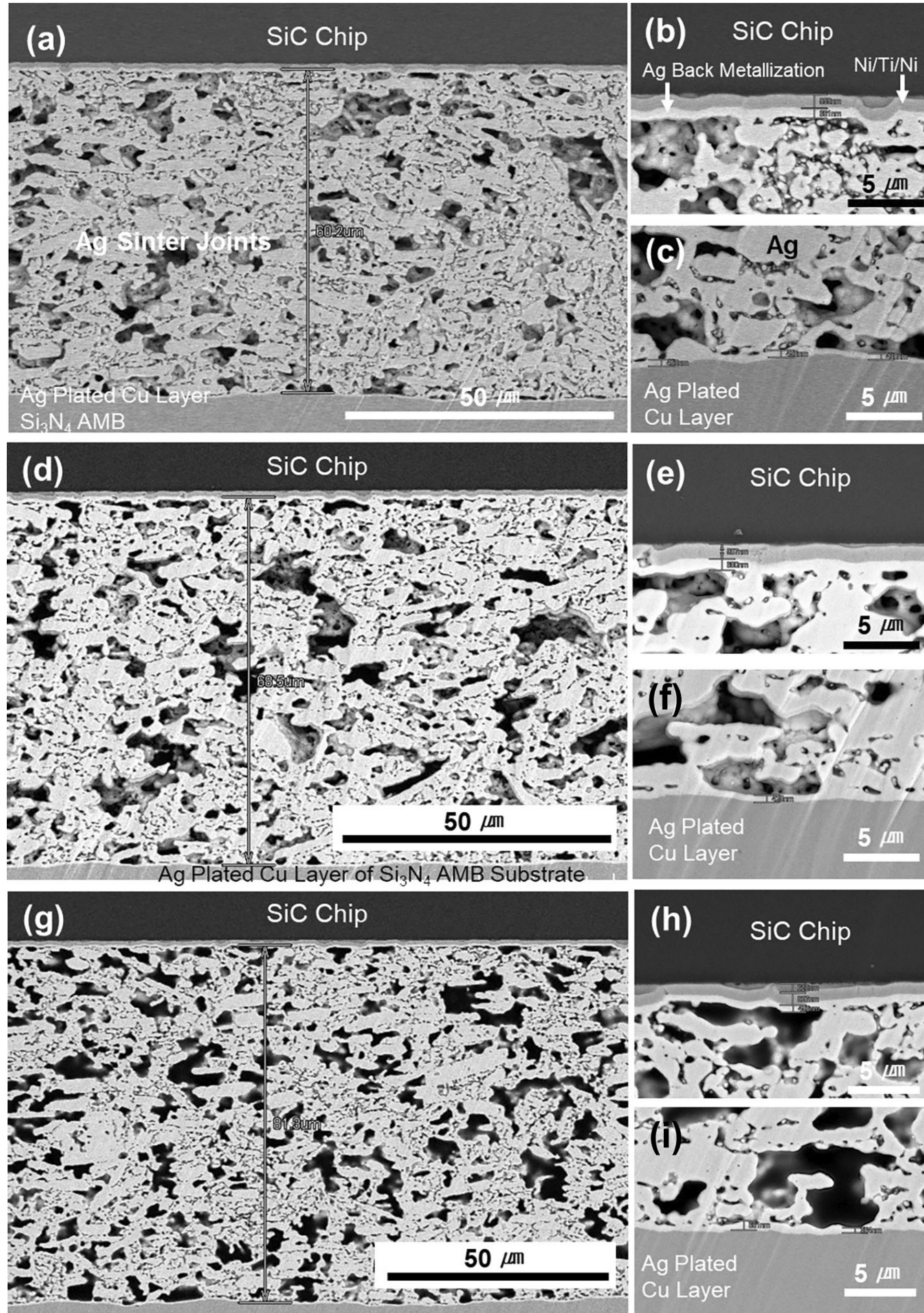

Fig. 8. SEM images of the Ag sinter joints of the 1200-V/200-A SiC MOSFET power module before and after the reliability tests: (a–c) as-sintered state, (d–f) after power cycling test for 1000 cycles, and (g–i) after the TCT for 500 cycles. Magnified SEM images of (b, e, h) the SiC chip side and (c, f, i) the Si_3N_4 AMB substrate side.

TCT. The microcracks were observed to occur at the triple bonding point of the grains. After a long time, these microcracks propagated inside the sinter joint, leading to a decrease in the bond strength.

The initial $R_{DS(ON)}$ of the 1200-V/200-A SiC MOSFET module was 6.60–6.99 mΩ. After the TCT and PCT, the $R_{DS(ON)}$ were 6.77–6.92 Ω and 6.63–6.97 Ω, respectively. These results indicated that, after the reliability test, the $R_{DS(ON)}$ was maintained constant during operation because the sinter joint was well maintained. The densifications after PCT and TCT were similar, and no cracks were observed. The PCT test conditions are more unfavorable for sinter joints than those of the TCT because the device is directly driven to apply heat. Therefore, the porosity and microstructures of the

sinter joints after the PCT test were slightly larger than before the test; however, the sinter joints were maintained. Therefore, the commercialization of SiC MOSFET modules without pressure sintering is considered feasible.

ACKNOWLEDGEMENTS

This research was supported by the Korea Evaluation Institute of Industrial Technology (KEIT) and the Ministry of Trade, Industry & Energy (MOTIE) of the Republic of Korea (No. 10063263). We thank Professor Yongil Kim of Sungkyunkwan University for his help with the power terminal bonding of the power module assembly.

REFERENCES

1. T. Kunimune, M. Kuramoto, S. Ogawa, T. Sugahara, S. Nagao, and K. Suganuma, *Acta Mater.* 89, 133 (2015).
2. R. Khazaka, L. Mendizabal, D. Henry, and R. Hanna, *IEEE Trans. Power Electron.* 30, 2456 (2015).
3. W.S. Hong, M.S. Kim, D. Kim, and C. Oh, *J. Electron. Mater.* 48, 122 (2019).
4. J. Biela, M. Schweizer, S. Waffler, and J. Kolar, *IEEE Trans. Ind. Electron.* 58, 2872 (2011).
5. Y. Gao, A. Huang, S. Krishnaswami, J. Richmond, and A. Agarwal, *IEEE Trans. Ind. Appl.* 44, 887 (2008).
6. C. Chen, Z. Zang, C. Choe, D. Kim, S. Noh, T. Sugahara, and K. Suganuma, *J. Electron. Mater.* 48, 1106 (2019).
7. H. Zhang, C. Chen, S. Nagao, and K. Suganuma, *J. Electron. Mater.* 46, 1055 (2017).
8. S.W. Yoon, M.D. Glover, and K. Shiozaki, *IEEE Trans. Power Electron.* 28, 2448 (2013).
9. C. Chen, D. Kim, Z. Wang, Z. Zhang, Y. Gao, and K. Suganuma, *Ceram. Int.* 45, 9573 (2019).
10. H. Zhang, W. Li, Y. Gao, H. Zang, J. Jiu, and K. Suganuma, *J. Electron. Mater.* 46, 5201 (2017).
11. H. Chin, K. Cheong, and A. Ismail, *Metall. Mater. Trans. B* 41, 824 (2010).
12. M.S. Kim, C. Oh, and W.S. Hong, *J. Weld. Join.* 37, 15 (2019).
13. Maruwa Co., LTD. www.maruwa-g.com/e/products/ceramic/ceramic-substrate-4.html. Accessed on 20th Jan 2019.
14. S. Noh, H. Zhang, and K. Suganuma, *Materials* 11, 2531 (2018).
15. K. Suganuma, S. Sakamoto, N. Kagami, D. Wakuda, K.S. Kim, and M. Nogi, *Micronelectron. Reliab.* 52, 375 (2012).
16. JEDEC Standard, JESD22-A122A, *Power Cycling* (JEDEC Solid State Technology Association, Arlington, VA, 2016).
17. W.S. Hong and S.S. Cha, *J. Microelectron. Packag. Soc.* 19, 67 (2012).
18. S. Divinski, M. Lohmann, and C. Herzig, *Acta Mater.* 49, 249 (2001).
19. J.S. Hirschhorn, *Introduction to Powder Metallurgy* (New York: The Colonial Press, 1969), pp. 155–273.
20. S.-K. Lin, S. Nagao, E. Yoko, C. Oh, H. Zhang, Y. Liu, S. Lin, and K. Suganuma, *Sci. Rep.* 6, 34769 (2016).
21. C. Oh, S. Nagao, T. Kunimune, and K. Suganuma, *Appl. Phys. Lett.* 104, 161603 (2014).
22. C. Oh, S. Nagao, and K. Suganuma, *J. Mater. Sci.: Mater. Electron.* 26, 2525 (2015).
23. R. Shioda, Y. Kariya, N. Mizumura, and K. Sasaki, *J. Electron. Mater.* 46, 1155 (2017).

Publisher's Note Springer Nature remains neutral with regard to jurisdictional claims in published maps and institutional affiliations.